

Ultrafast MHz-Rate Burst-Mode Pump–Probe Laser for the FLASH FEL Facility Based on Nonlinear Compression of ps-Level Pulses from an Yb-Amplifier Chain

Marcus Seidel,* Federico Pressacco,* Oender Akcaalan, Thomas Binhammer, John Darvill, Nagitha Ekanayake, Maik Frede, Uwe Grosse-Wortmann, Michael Heber, Christoph M. Heyl, Dmytro Kutnyakhov, Chen Li, Christian Mohr, Jost Müller, Oliver Puncken, Harald Redlin, Nora Schirmel, Sebastian Schulz, Angad Swiderski, Hamed Tavakol, Henrik Tünnermann, Caterina Vidoli, Lukas Wenthaus, Nils Wind, Lutz Winkelmann, Bastian Manschwetus, and Ingmar Hartl

The Free-Electron Laser (FEL) FLASH offers the worldwide still unique capability to study ultrafast processes with high-flux, high-repetition rate extreme ultraviolet, and soft X-ray pulses. The vast majority of experiments at FLASH are of pump–probe type. Many of them rely on optical ultrafast lasers. Here, a novel FEL facility laser is reported which combines high average power output from Yb:YAG amplifiers with spectral broadening in a Herriott-type multipass cell and subsequent pulse compression to sub-100-fs durations. Compared to other facility lasers employing optical parametric amplification, the new system comes with significantly improved noise figures, compactness, simplicity, and power efficiency. Like FLASH, the optical laser operates with 10-Hz burst repetition rate. The bursts consist of 800- μ s long trains of up to 800 ultrashort pulses being synchronized to the FEL with femtosecond precision. In the experimental chamber, pulses with up to 50- μ J energy, 60-fs full-width half-maximum duration and 1-MHz rate at 1.03- μ m wavelength are available and can be adjusted by computer-control. Moreover, nonlinear polarization rotation is implemented to improve laser pulse contrast. First cross-correlation measurements with the FEL at the plane-grating monochromator photon beamline are demonstrated, exhibiting the suitability of the laser for user experiments at FLASH.

1. Introduction

The superconducting Free-Electron Laser (FEL) FLASH provides ultrashort, extremely powerful pulses in the extreme ultraviolet (XUV) and soft X-ray spectral range (1.5–50 nm) at the highest repetition rates worldwide. Since more than 80% of the experiments at FLASH are time-resolved pump–probe experiments, femtosecond optical pulses constitute a vital cornerstone of contemporary FEL experiments. In particular, the plane-grating (PG) monochromator photon beamline at FLASH^[1–3] is constantly in high demand and was booked in each of the last four years for more than 50% of all science experiments using pump–probe lasers. The beamline serves predominantly the condensed matter science community using methods, such as time-resolved photoelectron, X-ray absorption, and X-ray emission spectroscopy which typically require

M. Seidel, F. Pressacco, O. Akcaalan, J. Darvill, N. Ekanayake, U. Grosse-Wortmann, M. Heber, C. M. Heyl, D. Kutnyakhov, C. Li, C. Mohr, J. Müller, H. Redlin, N. Schirmel, S. Schulz, A. Swiderski, H. Tavakol, H. Tünnermann, C. Vidoli, L. Wenthaus, L. Winkelmann, B. Manschwetus, I. Hartl
Deutsches Elektronen-Synchrotron DESY
Notkestraße 85, 22607 Hamburg, Germany
E-mail: marcus.seidel@desy.de; federico.pressacco@desy.de


T. Binhammer, M. Frede, O. Puncken
neoLASE GmbH
Hollerithallee 17, 30419 Hannover, Germany

C. M. Heyl
Helmholtz-Institute Jena
Fröbelstieg 3, 07743 Jena, Germany

C. M. Heyl
GSI Helmholtzzentrum für Schwerionenforschung GmbH
64291 Darmstadt, Germany

N. Wind
Physics Department University of Hamburg and Centre for Free-Electron Laser Science (CFEL)
22761 Hamburg, Germany

N. Wind
Ruprecht Haensel Laboratory
Deutsches Elektronen-Synchrotron DESY
D-22607 Hamburg, Germany

 The ORCID identification number(s) for the author(s) of this article can be found under <https://doi.org/10.1002/lpor.202100268>

© 2022 The Authors. Laser & Photonics Reviews published by Wiley-VCH GmbH. This is an open access article under the terms of the Creative Commons Attribution License, which permits use, distribution and reproduction in any medium, provided the original work is properly cited.

DOI: 10.1002/lpor.202100268

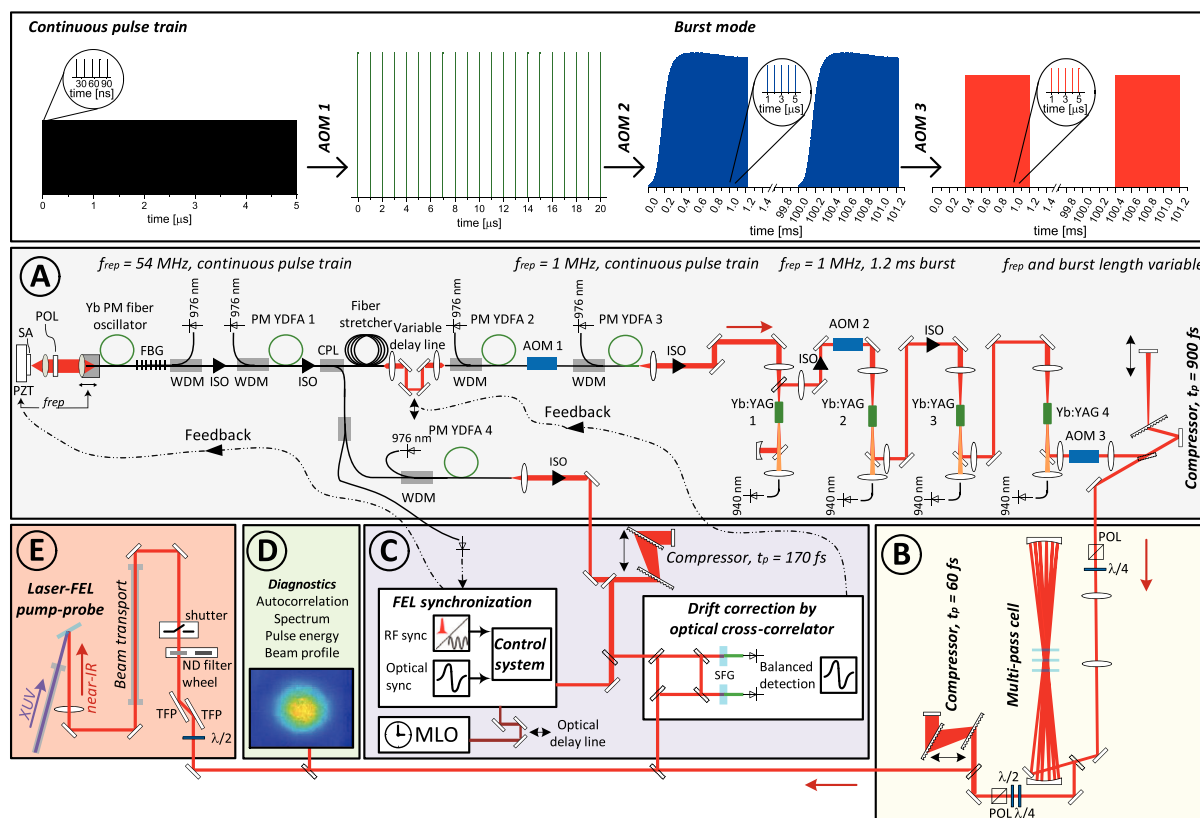


Figure 1. The top panel shows the pulse trains and burst shapes, respectively. The other panels give an overview of the laser setup consisting of five sections: A) Burst generation and amplification section consisting of a fiber oscillator with controlled cavity length, four fiber preamplifiers, four bulk Yb:YAG main amplifiers, three AOMs for burst preparation and shaping, a delay line for drift control and a fiber stretcher as well as a grating compressor for dispersion control. B) Pulse compression section consisting of an MPC, polarization optics and a grating compressor. C) Synchronization and timing section consisting of two balanced cross-correlators. D) Laser diagnostics section consisting of near- (shown beam profile) and far-field cameras, a spectrometer, an autocorrelator and an energy meter, E) – laser delivery section consisting of a variable attenuator and the beam transport unit to the PG beam line. Black solid lines denote fiber, red / orange solid lines denote free path optics, black dashed lines electrical signals. AOM – acousto-optic modulator, CPL – coupler, FBG – fiber Bragg grating, f_{rep} – repetition rate, ISO – optical isolator, MLO – main laser oscillator, ND – neutral density, POL – polarizer, PM – polarization maintaining, SA – saturable absorber, SFG – sum frequency generation, TFP – thin-film polarizer, t_p – pulse duration, WDM – wavelength division multiplexer, YDFA – Ytterbium-doped fiber amplifier

sub-100 fs pulses in the near-infrared spectral region for nonresonant sample excitation.

To enable FEL users to fully exploit their limited beam time, facility lasers must be operational 24/7. At FLASH, the availability of the optical lasers for pump-probe experiments was above 95% of the requested time over the past 3 years. To achieve such long-term performance, the lasers at FLASH host various online diagnostics and are to a large extent remotely controllable. Ultimately, excellent passive stability is desired which calls for simple and compact laser systems.

During the past ten years, two optical lasers were available at the FLASH1 beamlines:^[4] First, a Ti:sapphire laser with 10 Hz repetition rate providing mJ-level pulse energies. Second, a μ J-level laser based on optical parametric chirped pulse amplification (OPCPA). This source emitted bursts adapted to the FEL pulse sequence (cf. **Figure 1** top panel). FLASH operates in burst-mode with 10 Hz repetition rate. The 800 μ s long bursts are again comprised of femtosecond pulse trains with 1 MHz repetition rate. Laser emission adapted to this pulse sequence is hence ideal for applications. At the PG beamlines, the requested pulse en-

ergies are moderate, that is typically on the 1 μ J order, but the requested intraburst repetition rates are high, usually between 100 kHz and 1 MHz. This allows to take full advantage of the unique pulse rates of the FEL which enables photon-hungry applications at the beamline. The previously used, complex OPCPA system was decommissioned in fall 2020 and has now been replaced by a much simpler laser system which is reported here. It is the first optical laser in FEL beamline user operation which relies on the concept of nonlinear spectral broadening in Herriott-type multipass cells (MPC).^[5,6] The method enables compression of high-power ps-level pulses from Yb-based lasers to sub-100 fs duration with a compact setup, very good intraburst pulse energy flatness and excellent burst-to-burst energy stability. The reported system provides multi- μ J pulses at 1030 nm with durations down to 60 fs. It furthermore contains a pulse shaping unit for improved pulse contrast in a time window of interest for user experiments. A burst energy stability of 0.5% rms over 24 h is demonstrated which is an order of magnitude better than the stability of the previous burst-mode laser.^[4] Finally, extensive diagnostics combined with field-programmable gate arrays (FPGA) and pro-

grammable logic controllers (PLC) offer FEL users to monitor and control the laser parameters by means of DESY's accelerator control system. As a result, the laser described here provides a stable and reliable new workhorse for users of the PG beamlines at FLASH. It will be an essential ingredient for upcoming cutting-edge FEL experiments.

2. Laser Setup

The laser is installed in a 12 m² large so-called modular optical delivery station in the FLASH1 experimental hall. For the sake of clarity, the laser setup has been subdivided into five parts which are highlighted by different background colors in Figure 1.

2.1. Burst Generation and Amplification

In Section A, a soliton mode-locked Fabry–Pérot-type fiber oscillator generates ultrashort pulses.^[7] Those are amplified in three consecutive single-mode Yb-doped fiber amplifiers (YD-FAs). Subsequently, the ≈ 15 nJ pulses from the fiber frontend are amplified up to 200 μ J at the plateau of the laser bursts in four Yb:YAG end-pumped rods, that is about 200 W intraburst average power. The solid-state amplifier design is adapted from a four stage Nd:YVO₄ amplifier implemented at the European XFEL photocathode laser.^[8] The pulse energies can only be reached by chirped pulse amplification (CPA). Consequently, the pulses are stretched by a 200 m long fiber behind YDFA 1 and recompressed to about 900 fs by a 4-pass single-grating compressor. Section 1 furthermore contains 3 acousto-optic modulators (AOMs). They down-pick the pulse repetition rate and control the laser pulse intensities along the bursts as visualized in the top panel of Figure 1. Iterative learning control^[9] is applied to achieve constant pulse energies over the burst by means of feedback to the AOM 3 modulation port. AOM 3 also sets the pulse repetition rate within the 800 μ s long burst according to user demands. The maximum of 1 MHz matches the FEL pulse rate. The fiber frontend has a second output behind YDFA 4. Short pulses (170 fs) at the oscillator's repetition rate (54 MHz) are generated to synchronize the optical pulses with the FEL bursts. The footprint of section A is only about 2 \times 0.7 m². More details are provided in the Supporting Information 1.

2.2. Pulse Compression

To increase the temporal resolution of the FEL pump–probe experiments, spectral broadening in a Herriott-type MPC and consequent pulse shortening in a grating compressor was used (Figure 1B). Whereas the majority of reported experiments rely on a single Kerr medium within the MPC, a hybrid multipass multiplate approach was implemented.^[10] By this method, the hitherto published femtosecond pulse compression factors from a single bulk MPC^[11–13] were clearly surpassed. Three 1 mm thin antireflection (AR) coated silica plates with 3 cm spacing were placed in the center of an about 350 mm long MPC. For maximized spectral broadening to a 55 fs Fourier transform limit, about 80% of the 115 μ J input pulse energy was transmitted through the output polarizer after 31 roundtrips. The pulses were compressed

by a record-high factor of more than 15 with a motor-controlled double-pass grating stage. Figure 2a,b show the retrieval results of a scanning frequency-resolved optical gating (FROG) measurement. The retrieved spectrum agrees well with the one measured in parallel with a commercial grating spectrometer, indicating the reliability of the FROG result. Moreover, high spectral homogeneity over the beam profile (Figure S3, Supporting Information) was obtained which is in good agreement with previous bulk-MPC experiments.^[11,14] The pulses were nearly Fourier-transform limited but clearly show side lobes, owing to the modulated spectrum. Figure 2c displays the compression quality in terms of pulse energy in the main peak and amplitude of the dominant side peak. The quantities were measured at different intraburst delays. This was possible by means of the modulation capabilities of AOM 3 which cut out single pulses from the burst. The relative pedestal amplitude was considered as the most critical parameter for FEL experiments. It amounts to about 10% of the main peak and is therefore comparable to the pulse-energy fluctuations in the FEL burst.^[15] The variations of the pulse shapes over the burst stemmed from the transient thermal lenses which are described in the Supporting Information 1.2. It is remarkable that the 30% waist area variation measured in the M²-meter results in only about 3.5 fs pulse duration variation over the burst (Figure 2d) which hardly affects the temporal resolution of the pump–probe-experiments at the PG beamline (Section 3).

A 24 h measurement was taken to investigate the stability of the nonlinearly broadened spectra (Figure 2f). Hardly any fluctuations are visible by eye. To quantify the stability, the Fourier transform limit within a 30 dB dynamic range was evaluated for each recorded spectrum, resulting in a standard deviation of only 0.4 fs at a 55.5 fs mean transform limit. This is on the subpercent level of the temporal resolution attained by optical pulse – XUV FEL cross-correlation measurements.

Pulse pedestals inherently emerge from the input pulse shape after the amplifier shown in Figure S1 (Supporting Information) and the self-phase modulated spectra.^[16] To suppress them, additional quarter-wave plates were placed at the entrance and the exit of the MPC. By introducing a slight polarization ellipticity with the entrance waveplate, the output polarization became intensity-dependent. Consequently, the polarizing beam splitter at exit of the MPC served as an artificial saturable absorber. This technique, called nonlinear polarization ellipse rotation, was previously used for pulse cleaning in fiber, single-pass nonlinear media and multipass geometries.^[17–19] Just recently, the application of the method to Herriott-type MPCs has also been theoretically studied.^[20] Here, it was for the first time directly integrated in an MPC-based spectral broadening setup. Pulse cleaning was introduced to suppress the postpulse delayed by 900 fs from the main peak (Figure 2e, black solid line) because of its signature in a cross-correlation measurements with the FEL (Supporting Information S6). Employing nonlinear polarization ellipse rotation suppressed the satellite pulse by more than an order of magnitude (Figure 2e, blue solid line). To accomplish this, both waveplates were manually adjusted such that the modulations of the spectrum after the MPC were minimized. The used configuration sufficed to quench the spurious signal emerging from the satellite pulse in FEL cross-correlation measurements (Section 3). The introduction of an artificial saturable absorber by the

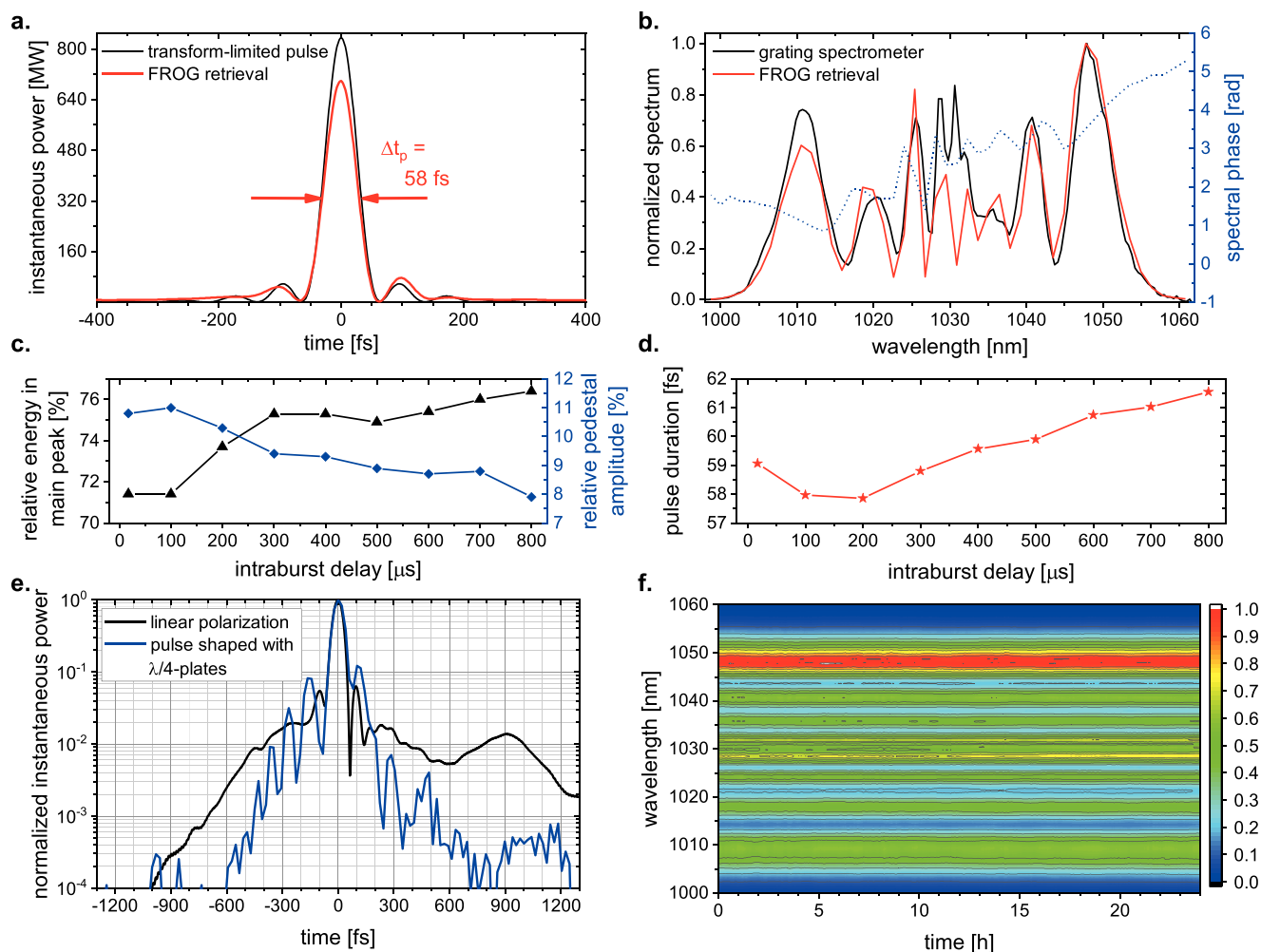


Figure 2. a) Retrieved FROG trace for 100 μs intraburst delay and comparison to the Fourier-transformed pulse derived from the retrieved spectrum shown in b) The spectral phase and a comparison to a spectrum directly measured with a grating spectrograph are shown as well. c) Compression quality evaluated in terms of relative energy in the main peak defined by the minima around ± 60 fs and in terms of relative pedestal amplitude, that is peak power of the pedestal around 100 fs divided by the peak power of the main pulse. d) Varying pulse durations over burst length. The spread is about 3.5 fs, that is less than 7% of the mean. e) Retrieved pulse from subplot a) shown in logarithmic scale (black line) and compared to retrieved pulse after introducing nonlinear polarization rotation in the MPC. f) Logged normalized spectra measured over 24 h every 10 s. The mean Fourier transform limit is 55.5 fs, its standard deviation 0.4 fs.

ellipse rotation method reduced the mean pulse energy at the diagnostics section by 39% to 35 μJ and increased the pulse width to about 70 fs owing to the polarization dependence of the nonlinear refractive index. Both drawbacks are however irrelevant for most of the user experiments which run at a few μJ pulse energy and with > 100 fs temporal resolution owing to the XUV-pulse stretching by the FEL beamline monochromator.

The footprint of Section B is about $0.3 \times 0.9 \text{ m}^2$. Consequently, the whole pulse generation and shortening unit covers only an area of less than $2.5 \times 1 \text{ m}^2$, and is thus considerably more compact than the previous OPCPA laser system.

2.3. Synchronization and Timing

A major task to ensure high time resolution of FEL-optical laser experiments is to synchronize both sources while providing pre-

cise control over their relative arrival time at the experiment. Therefore, the laser system includes two balanced optical cross-correlators^[21,22] which are located in section C of the setup in Figure 1 and explained in more detail in the Supporting Information 5. One cross-correlator is used for locking the fiber oscillator repetition rate to a main laser oscillator (MLO) operating at 1550 nm central wavelength. This facility-wide timing reference is distributed via length-stabilized fibers.^[22] To minimize the cross-correlator's error signal a piezo-actuated end-mirror of the laser cavity is controlled to adjust the oscillator repetition rate. The control electronics are based on the MicroTCA4 platform developed at DESY^[23] and a programmable FPGA hosting fast feedback loops. Since the capture range of the optical synchronization method is limited to about 400 fs, the fiber oscillator repetition rate is prestabilized by conventional RF phase-locking.^[22] The 54 MHz pulse train from the auxiliary fiber frontend output is used in both cross-correlators. Whereas it is stabilized in

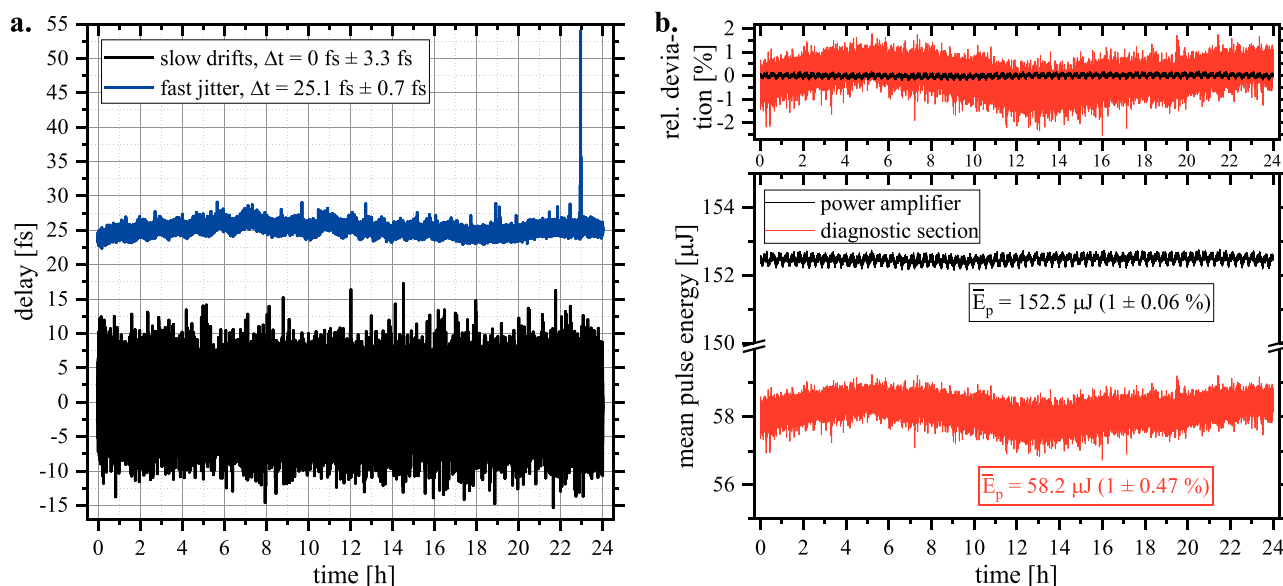


Figure 3. a) Pulse arrival time delay measurements in both balanced cross-correlators recorded in parallel to the energy stability in b) The blue line shows the fast jitter derived from the 54 MHz pulse trains. The black line shows the in-loop drift measurement of the 10 Hz laser bursts after nonlinear pulse compression. b) Energy stability measured over one day of user beamtime with a 1 Hz rate by photodiodes behind the main amplifier (black solid lines) and in the diagnostics section (red solid lines). The lower panel shows the absolute mean pulse energies inside the laser bursts, the upper panel shows the relative standard deviations from the mean value. The Yb:YAG amplifier is highly stable with $< 0.1\%$ standard deviation, the MPC output shows also a low relative standard deviation of less than 0.5% .

the first cross-correlator, it is used as reference in the second correlator measuring slow timing drifts of the pulses coming from the MPC. A motor-controlled translation stage located in the fiber front-end serves as variable delay line to compensate for the measured drifts. The residual timing instability was logged over a 24 h period during a user campaign (Figure 3a). The fast jitter derived from the 54 MHz pulse train was on average 25.1 fs within a 10 Hz to 1 MHz bandwidth. Only four out of $> 85\,000$ logged data points exhibited more than 30 fs timing-offset. In addition, more than 99.5% of the slow drifts measured in the second cross-correlator were within a ± 10 fs range and never exceeded a 20 fs absolute timing offset. Consequently, the total jitter between pump-probe laser and optical main oscillator is clearly below the > 100 fs temporal resolution achievable at the monochromator beamlines and thus hardly contributes to the overall resolution (Figure 4; and Figure S8, Supporting Information).

2.4. Laser Stability

Figure 1d hosts various diagnostic tools to measure pulse spectra, energies, durations, and beam profile as well as position. The burst energy stability is continuously logged with a 1 Hz rate by the accelerator control system. Figure 3b shows the logged pulse mean energies at the diagnostics section. The energies are averaged over all pulses of the bursts. The data were recorded in parallel to the synchronization data shown in Figure 3a. With less than 0.1% relative standard deviation, the solid-state amplifier exhibits a highly stable output. The burst energy fluctuations behind the MPC are higher but still below 0.5% which is an order of magnitude better than the reported value for the previously used OPCPA system.^[4] In parallel, beam displacement and pointing

was analyzed in the same 1 day measurement period at the diagnostics section. The standard deviations of the positions were 4.4 and $6.9 \mu\text{m}$ in x- and y-direction, respectively. This corresponds to 0.5% of the $1/e^2$ -beam radius in x- and 1.0% in y-direction. The pointing standard deviations were 2.0 and $2.6 \mu\text{rad}$ in x- and y-direction, respectively. The measurement data are shown in Figure S4 (Supporting Information). Users have not observed any problems with pointing during the first campaigns with the laser. It is to note that at present, the long-term stability strongly depends on the temperature and humidity stability of the FLASH experimental hall where the laser is installed without distinct air conditioning. The Supporting Information S4.2 shows the mutual dependence of temperature, humidity, and mean pulse energy at the diagnostics section.

2.5. Automation and Controls

In order to rapidly adjust the laser settings to the user needs, to prevent drifts or damages, to minimize downtime, and to continuously record pulse and beam parameters, the laser system is to a large degree remotely controllable and uses several automation routines. For this purpose, it has been integrated into the FLASH facility control system.^[24,25]

The pulse trains are monitored by means of InGaAs photodiodes behind the oscillator, each fiber and solid-state amplifier, the fiber stretcher, the AOMs 1 and 3, at the compressor and MPC inputs, at the diagnostics section, and the incoupling to the beamline. Pulse spectrum and autocorrelation as well as the near- and far-field beam profiles at the stabilization units behind the main amplifier and in the diagnostics section are continuously recorded. The MPC is equipped with three additional cameras

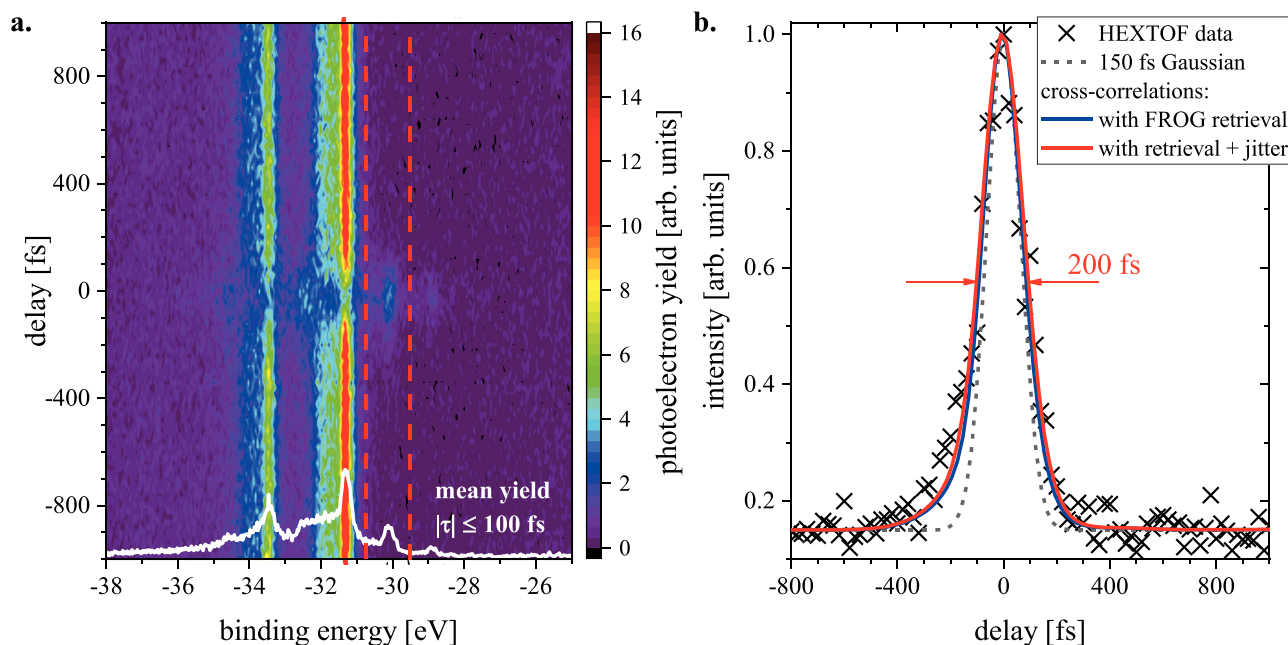


Figure 4. a) Measured photoelectron spectra of the W(110) 4f core level as function of time delay between optical laser and FEL ($h\nu_{\text{FEL}} = 112 \text{ eV} \approx 93 \times h\nu_{\text{nIR}}$). At delays larger than $|\pm 600 \text{ fs}|$, the binding energies virtually represent the steady state of the 4f core level. On contrary, for delays within $\pm 100 \text{ fs}$ (white solid line), optical photon dressed states emerge separated by multiples of $\pm h\nu_{\text{nIR}}$. They are visible up to the 2nd order near -28.9 eV . Clearly most prominent is the single-photon side-band at $E_{b,1} + h\nu_{\text{nIR}} \approx -30.1 \text{ eV}$. The integrated photoelectron yield in a range of 1.25 eV around this band (red dashed lines) yields the cross-correlation measurement of b). The integrated data points are represented by the black crosses. Moreover, the cross-correlation was modeled by Equation (1) based on the FROG retrieval of the optical pulse. The blue solid line shows the expected cross-correlation excluding timing jitter between the FEL and optical pulses. The red line additionally considers jitter of 30 fs rms . For comparison, the estimated FEL pulse is shown (gray dashed line) which mainly determines the temporal resolution of the experiment. No side lobes emerge in the cross-correlation.

for input- and output-beam profile and scattering light monitoring. If one of the Kerr media gets damaged, it can be replaced remotely by a slider which has however not been necessary, yet. The main amplifier Yb:YAG crystals are protected by an FPGA-based system which immediately interrupts the trigger to the pump diodes' power supply if a single seed pulse is missing in the burst or if the pulse energy drops below a set threshold value. The triggers of all photodiodes and measurement devices can be remotely controlled by laser experts who can also turn on and off all stages of the laser system remotely and synchronize it to the main laser oscillator. Moreover, the laser bursts after AOM 3 can be arbitrarily shaped and the intraburst pulse repetition rate can be set (Supporting Information S1.2). Finally, the pulse entering the MPC can be prechirped by the motorized grating stage in front of it.

Additionally, users of the PG beamline have several control options that fulfill their most common requests. First, the final Figure 1e contains a motor-controlled shutter and a variable attenuator unit. The pulse energies are adjusted by set of reflective neutral density filters and by a rotatable waveplate in front of two thin-film polarizers, resulting in 57.5 dB dynamic range. The burst energies can be directly measured by a pyroelectric energy meter addressable through a motorized flip mirror. Second, a high-precision, low drift translation stage is implemented for delaying the $1.55 \mu\text{m}$ reference beam (Figure 1c). It is used to control the relative delay between the FEL and the optical pulses. An automated routine, which shifts the overall laser timing up to several milliseconds, initiates the temporal overlap between

pump and probe pulses. Third, users can vary the duration of the optical pulses by changing the step motor-controlled grating separation in the compressor behind the MPC. Finally, the polarization of the light and the position of the beam in the experimental chamber is adjustable.

3. Free-Electron Laser Pump–Probe Experiment

Figure 4 shows the results of a proof-of-concept pump–probe experiment at the PG beamline. Optical and free electron lasers were overlapped at the surface of a tungsten sample to measure their cross-correlation signal.^[26,27] The HEXTOF detection scheme^[15] was used to collect the photoelectron yield in dependence of free electron kinetic energy and FEL-optical pulse delay. Figure 4a resolves the vicinity of the W(110) 4f core-level binding energies at $E_{b,1} \approx -31.3 \text{ eV}$ and $E_{b,2} \approx -33.4 \text{ eV}$. Separated by multiples of the optical photon energy $h\nu_{\text{nIR}} = 1.2 \text{ eV}$, transient dressed-states are formed symmetrically around the core-levels.^[28,29] Consequently, integration over the energy range of 1.25 eV around $E_{b,1} + h\nu_{\text{nIR}}$ yields the FEL-optical laser cross-correlation signal.^[30] Figure 4b shows the normalized data of the cross-correlation measurement and compares it to numerical calculations applying the equation

$$I_{\text{XC}}(\tau) \propto \int dt_0 P(t_0) \int dt I_{\text{FEL}}(t, t_0) I_{\text{nIR}}(t + \tau) \quad (1)$$

Where the normal distribution $P(t_0) = (2\pi\sigma_0^2)^{-1/2} \exp\{-t_0^2/(2\sigma_0^2)\}$ with $\sigma_0 = 30 \text{ fs}$ accounts for tim-

ing jitter, $I_{\text{FEL}}(t, t_0)$ is the FEL pulse intensity, and $I_{\text{nlr}}(t + \tau)$ is the retrieved FROG pulse from Figure 2e. The FEL pulse was approximated by a Gaussian $I_{\text{FEL}}(t, t_0) \propto \exp\{-4\ln 2(t - t_0)^2 / \Delta t_p^2\}$ where the full-width half-maximum (FWHM) duration Δt_p was derived from electron bunch streaking experiments^[31] and the plane grating illumination (Experimental Section). Since the electron bunch distribution was not Gaussian, this is a coarse estimation. Nevertheless, the agreement between the measured data and the computed curve is good. The 200 fs width of the cross-correlation is mainly determined by the 150 fs FEL pulse duration. The optical pulse adds about 45 fs to it. The impact of the 30 fs rms jitter is very small. In order to study the best temporal resolution at the PG beamline, shorter FEL pulses must be generated. This will be subject to an upcoming study. The cross-correlation trace exhibits broader wings than a Gaussian of comparable width. This originates at least to some degree from the pedestals of the optical pulse at ± 100 fs (Figure 2e). Those are smeared out by the longer FEL pulses. Contrary to the cross-correlation measurement with the optical pulses shown in Figure 2a (Supporting Information 6), no satellite pulses are visible in the cross-correlation.

4. Discussion

Efficient nonlinear pulse compression allows to take advantage of high-power Yb-ion based lasers without compromising temporal resolution. This promises a significant boost of on-target laser fluence in FEL pump–probe experiments, and thus constitutes a crucial building block of the FLASH 2020+ upgrade which targets THz to UV spectral coverage by optical lasers.^[32] Precedent experiments with MPCs at FLASH have already demonstrated the potential of nonlinear pulse compression at FEL facilities.^[33,34] Here, the first laser system is reported which fully relies on the spectral broadening concept and has been employed in FEL user experiments.^[35] To date, PG beamline users have given positive feedback to the novel pump laser system.

In contrast to the previous OPCPA concept,^[4] the system reported here exhibits various advantages: First, the order-of-magnitude energy stability improvement implies a clear reduction of measurement noise and reduced need for averaging, respectively. Pulse-to-pulse energy fluctuations are second also improved by active burst flattening through the last AOM in the amplifier unit. Such flattening was not possible in the OPCPA setup due to the a priori sub-100 fs bandwidth of the parametric amplifier seed. Third, the new system delivers up to 800 pulses per burst corresponding to the number of FEL pulses arriving at the experimental chamber. The previous system could lately deliver only 400 pulses per burst in best case.^[15] The spectral broadening-based system can hence improve the data acquisition rate by a factor of two. Eventually, the much better power-efficiency, the simplicity and the compactness of the system reported here promises reliable continuous operation without the need for expert intervention during user campaigns.

On the one hand, the demonstrated FWHM pulse duration of 60 fs is clearly shorter than the durations reported from the OPCPA system.^[4,15] On the other hand, the main drawback of the nonlinear pulse compression approach is the modest pulse contrast. It is, without further measures, intrinsically limited by

the self-phase modulated spectrum as Figure 2a implies. Furthermore, the output pulse shape of the laser amplifier caused additional temporal side lobes. The applied nonlinear ellipse rotation method is very simple to implement because it only requires additional waveplates in the MPC. It has proven as an excellently suited technique to suppress spurious FEL pump–probe signals originating from laser pulse pedestals. The method is clearly more efficient than the cross polarized wave (XPW) generation^[36] or the OPCPA approach which are also used for contrast enhancement. Moreover, the instantaneous nature of the exploited Kerr nonlinearity enables suppression of both pre- and postpulses which is vital for pump–probe experiments. The relaxation time of alternatively used real saturable absorbers^[37] or plasma mirrors^[38] precludes the suppression of postpulses on a sub-ps time scale. The drawback of the nonlinear ellipse rotation method is that to some extent pulse energy and duration are compromised. The increase of pulse duration stems from the reduced nonlinear refractive index for elliptical polarization.^[39] It could be compensated by tighter focusing as the Kerr-media damage threshold is also polarization-dependent. For the FEL-pump–probe experiments, it is however more important to have a flexible intensity filter that can be adapted to the observed dynamics under test. In the reported example, the pedestal around 900 fs delay was clearly visible, whereas the side peaks around 100 fs delay had only a minor impact on the cross-correlation trace. If shorter FEL pulses are used to monitor ultrafast dynamics, the ellipse rotation method should be optimized for suppressing the 100 fs delay pedestals. The cleaning method is tunable through the initial ellipticity. Energy losses are inevitable because the cleaning technique introduces an artificial saturable absorber in the beam path. But the energy efficiency is not critical for the FEL beamline because most user experiments run at low μJ pulse energies. That is clearly less than the 35 μJ pulse energy measured in the diagnostics section after cleaning. It is to note that the waveplate settings were found empirically by observing the modulation depth of the output spectrum. A theoretical investigation of the method for spectral broadening in hollow-core capillaries^[40] shows that efficiency as well as contrast can be further improved by a systematic study of the output pulse shape in dependence of polarization ellipticity in the MPC. The measured 30 dB contrast was however sufficient for all user experiments which have been conducted so far. Moreover, it should be noted that the efficiency of the method also depends on the shape of the pulses entering the MPC and the targeted pulse shape. In the present study, mainly the side lobes of the amplifier pulses were suppressed, not primarily the pedestals introduced by self-phase modulation.

The need for only modest pulse energies results in the most compact, cost-efficient, and least intensity-noisy near-infrared FEL pump–probe laser among the previously reported ones.^[41–44] Only the OPCPA-based laser at LCLS shows comparable long-term pulse energy stability if it is driven with reduced pump power.^[41] At full pump power, the LCLS system provides up to 90 W average power after the OPCPA, that is conversion of about 13.5% of the power provided by the Yb:YAG amplifier. By contrast, the system reported here can exploit about 50% of the pulse energy available after the chirped pulse amplifier. Only 20% of the losses stem from the MPC. The main loss source is the flexible grating compressor which could be replaced by efficient disper-

sive mirrors. Consequently, even compression to the 10 fs-level in a dual stage scheme^[33] is expected to be significantly more efficient than the established OPCPA technique. The results presented here highlight the attractiveness of the pulse-compression approach for future FEL pump–probe laser developments. Its scalability to kW average power and pulse energy levels exceeding 100 mJ has just recently been demonstrated.^[45,46]

The about 30 fs rms timing jitter may be further reduced with a recently developed nonlinear amplifying loop mirror (NALM) laser oscillator.^[47] The jitter refers to the locking of the optical laser to the main laser oscillator. The actual timing instability between FEL and optical pulses may be slightly larger.^[22] Simultaneous arrival time monitoring of pump and probe could be used to attain precise timing information.^[48] The method applied to the European hard X-ray FEL is however difficult to implement for FLASH's XUV to soft-X-ray spectral coverage.^[22] The burst-to-burst timing fluctuations of about 20 fs (Figure 3a) correspond to the upper limit of the slow jitter introduced by the long beam path in the MPC. The timing stability of facility OPCPAs^[41–43] were not characterized with a similar cross-correlator. But they exhibited comparable or even larger fluctuations when the relative optical and FEL pulse arrival times^[48] or the seed and pump pulse jitters were measured.^[41] This suggests that the MPC concept does not impede precise synchronization of pump and probe pulses. By contrast, the single path setup reduces synchronization complexity and eliminates central wavelength instabilities.^[41] This and the very good energy stability enable in turn precise calibration of the drift correlator (Figure S7, Supporting Information), and thus exact postcorrection of timing fluctuations in pump–probe experiments. In the experiments reported here, the 30 fs rms timing jitter had hardly any impact on the temporal resolution since the FEL pulses were comparably long at the monochromator beamline. Therefore, the possible improvements in synchronization and absolute jitter characterization will not lead to significant changes of the temporal resolution but rather present an interesting development direction for other beamlines.

Whereas the previous OPCPA system was generating pulses at 800 nm central wavelength, the spectra of the pulses from the laser reported here are centered at 1030 nm. As the sample excitation in the user experiments is typically nonresonant, this wavelength shift does not influence the usability of the laser. Recently, an additional harmonic generator delivering light at 517 nm has been implemented (Supporting Information S7). The intensity dependence of the nonlinear frequency conversion additionally cleans the ultrashort pulses as the smooth spectrum of the second harmonic indicates (Figure S10b, Supporting Information). The third harmonic at 343 nm will be available to the users in the near future which will further extend the applicability of the new laser system.

5. Conclusion

A first FEL facility laser was presented which fully relies on the spectral broadening in a multipass cell approach. The demonstrated compression factor of 15 to FWHM durations of 60 fs makes it possible to exploit the stability, compactness, and efficiency of a high-power Yb:YAG laser emitting ps-level pulses. The short pulse durations in combination with the about 30 fs

rms timing jitter are excellently suited for pump–probe experiments at the FLASH PG beamline where temporal resolution is limited by the FEL monochromator. A major challenge of nonlinear pulse compression methods, to generate clean pulses, was tackled by the nonlinear ellipse rotation method which led to a significant reduction of spurious signals in FEL cross-correlation measurements. In conclusion, the new compact and stable facility laser for pump–probe experiments at FLASH meets all major user requirements, promises high reliability during 24/7 operation and will certainly contribute to upcoming cutting-edge ultrafast science experiments at the PG beamlines at DESY's FEL facility.

6. Experimental Section

FROG Measurements: A commercial scanning second-harmonic FROG was used (Mesa Photonics). It contained a 20 μm thin BBO crystal for nonlinear frequency conversion. A beam sampler after the grating compressor was inserted to direct the beam to the measurement device. AOM 3 was used to reduce the number of pulses from 800 to 5 which illuminated the spectrometer in the FROG test. By delaying the trigger of AOM 3 intraburst delay dependent FROG measurements were done. A 512×512 grid was chosen. The FROG errors varied between 0.23% and 0.68%. A grating spectrum was measured in parallel by collecting scattered light from the block of the main beam.

M²-Measurements: A commercial M²-meter was used (Spiricon M200-s) to determine M². The device uses the 4 σ -method, automatically attenuates and calculates the region of interest of the camera image. By means of a beam sampler, light in front of the MPC or after the MPC was steered to the measurement device. The beam camera was triggered and the integration time was set to 40 μs . This allowed to measure M² at different intraburst delays.

Laser Stability Measurements: InGaAs photodiodes were used to continuously track laser pulse energies at different parts of the setup. The sampled laser beam was strongly attenuated and focused onto the detector area to reduce beam pointing artifacts. The pulse energies were calibrated by comparing the integrated voltage over one burst with the burst energy measured by a commercial energy meter. From the integrated voltage of a single pulse, the pulse energy was then retrieved. The pulse energies shown in Figure 3b were derived from diodes located directly behind the beam stabilization units to minimize fluctuations caused by beam pointing.

Optical Cross-Correlator Calibration: To calibrate the optical cross-correlator for drift correction, a delay scan was done (Figure S7, Supporting Information) and the slope of the balanced photodiode signal with respect to the displacement of the variable translation stage was fitted. For the optical locking of the laser oscillator, the phase of the RF-lock was shifted. The recorded balanced signals were then converted to fs delays.

Measurements with the HEXTOF Instrument at the FLASH1 PG2 Beamline: The monochromatic FEL and optical laser beams impinge on the sample in a collinear configuration thanks to a plane holey mirror in the incoupling section of the beamline, 1.5 m upstream of the sample. The incident angle of the two beams was 68 degree (with respect to sample normal). The focus sizes of the FEL and the optical laser beam were 150 × 300 μm^2 and 200 × 400 μm^2 , respectively. The FEL photon energy was $h\nu_{\text{FEL}} = 112$ eV ($\lambda = 11$ nm). The FEL pulses contained a few thousand photons for core-level spectroscopy.^[15] The near-infrared pulse energies were 2.0 μJ , corresponding to 73 GW cm⁻² peak intensity and 6.4 mJ cm⁻² peak fluence, respectively. The bursts contained 480 pulses. The photoelectrons were collected by the HEXTOF extractor lens and parallelized onto a multichannel plate for momentum and delay detection.^[15] Figure 4 shows momentum-integrated data after 30 min of averaging. The sample was contaminated with carbon atoms as the usual annealing treatment was skipped for the shown measurement run. The HEXTOF detection scheme allows to collect all electrons emitted above the sample surface giving an effective acceptance angle of 2 π steradians.

FEL Pulse Duration Estimation: As the direct measurement of the high energy FEL pulses is difficult, the electron bunches were analyzed in order to estimate the photon pulse durations. A LOLA-type transverse deflecting radio-frequency structure was used to measure the longitudinal electron bunch profile. Its rms duration corresponds roughly to the FWHM of the FEL pulses if the profile is Gaussian.^[31] This estimation results in a 120 fs pulse width. The 150 fs duration used in the model is additionally taking into account a 30 fs pulse elongation induced by the plane grating monochromator of the beamline. The elongation was calculated from the XUV beam size on the grating and its line density.^[15]

Supporting Information

Supporting Information is available from the Wiley Online Library or from the author.

Acknowledgements

The authors acknowledge DESY (Hamburg, Germany), a member of the Helmholtz Association HGF, for the provision of experimental facilities. Parts of this research were carried out at FLASH. The authors thank Holger Meyer and Sven Gieschen from the University of Hamburg for support of the HEXTOF instrument. They also acknowledge their colleagues from European XFEL for developing and sharing the drift cross-correlator design D:K., M.H., N.W. acknowledge funding by the DFG within the framework of the Collaborative Research Centre SFB 925 - 170620586 (project B2).

Open access funding enabled and organized by Projekt DEAL.

Conflict of Interest

The authors declare no conflict of interest.

Data Availability Statement

The data that support the findings of this study are available from the corresponding author upon reasonable request.

Keywords

high-power lasers, lasers for facilities, pulse compression, pump–probe, spectral broadening, synchronization, ultrafast lasers

Received: May 20, 2021

Revised: September 28, 2021

Published online: January 18, 2022

- [1] M. Martins, M. Wellhöfer, J. T. Hoeft, W. Wurth, J. Feldhaus, R. Follath, *Rev. Sci. Instrum.* **2006**, 77, 115108.
- [2] N. Gerasimova, S. Dzierzhytski, J. Feldhaus, *J. Mod. Opt.* **2011**, 58, 1480.
- [3] The PG beamlines at FLASH1, https://photon-science.desy.de/facilities/flash/beamlines/pg_beamlines_flash1/index_eng.html (accessed: December 2021).
- [4] H. Redlin, A. Al-Shemmary, A. Azima, N. Stojanovic, F. Tavella, I. Will, S. Düsterer, *Nucl. Instrum. Methods Phys. Res., Sect. A* **2011**, 635, S88.
- [5] J. Schulte, T. Sartorius, J. Weitenberg, A. Vernaleken, P. Russbuehlt, *Opt. Lett.* **2016**, 41, 4511.
- [6] M. Hanna, X. Délen, L. Lavenue, F. Guichard, Y. Zaouter, F. Druon, P. Georges, *J. Opt. Soc. Am. B* **2017**, 34, 1340.

- [7] I. Hartl, G. Imeshev, L. Dong, G. C. Cho, M. E. Fermann, *CLEO Conf. Lasers Electro-Opt.*, Vol. 3, IEEE, Baltimore, MD **2005**, pp. 1641–1643.
- [8] L. Winkelmann, A. Choudhuri, U. Grosse-Wortmann, I. Hartl, C. Li, C. Mohr, J. Müller, F. Peters, S. Pfeiffer, S. Salman, in *Proc. 39th Free Electron Laser Conf. FEL2019*, JACoW Publishing, Hamburg, Germany, **2019**, p. 4.
- [9] S. Arimoto, S. Kawamura, F. Miyazaki, *J. Robot. Syst.* **1984**, 1, 123.
- [10] M. Seidel, P. Balla, T. Binhammer, M. Frede, G. Arisholm, L. Winkelmann, I. Hartl, C. M. Heyl, *EPJ Web Conf.* **2020**, 243, 21001.
- [11] J. Weitenberg, A. Vernaleken, J. Schulte, A. Ozawa, T. Sartorius, V. Pervak, H.-D. Hoffmann, T. Udem, P. Russbuehlt, T. W. Hänsch, *Opt. Express* **2017**, 25, 20502.
- [12] S. Gröbmeyer, K. Fritsch, B. Schneider, M. Poetzlberger, V. Pervak, J. Brons, O. Pronin, *Appl. Phys. B* **2020**, 126, 159.
- [13] J. Song, Z. Wang, R. Lv, X. Wang, H. Teng, J. Zhu, Z. Wei, *Appl. Phys. B* **2021**, 127, 50.
- [14] N. Daher, F. Guichard, S. W. Jolly, X. Délen, F. Quéré, M. Hanna, P. Georges, *J. Opt. Soc. Am. B* **2020**, 37, 993.
- [15] D. Kutnyakhov, R. P. Xian, M. Dendzik, M. Heber, F. Pressacco, S. Y. Agustsson, L. Wenthaus, H. Meyer, S. Gieschen, G. Mercurio, A. Benz, K. Bühlman, S. Däster, R. Gort, D. Curcio, K. Volckaert, M. Bianchi, C. Sanders, J. A. Miwa, S. Ulstrup, A. Oelsner, C. Tusche, Y.-J. Chen, D. Vasilyev, K. Medjanik, G. Brenner, S. Dzierzhytski, H. Redlin, B. Manschwetus, S. Dong, et al., *Rev. Sci. Instrum.* **2020**, 91, 013109.
- [16] A.-L. Viotti, S. Alisauskas, H. Tünnemann, E. Escoto, M. Seidel, K. Dudde, B. Manschwetus, I. Hartl, C. M. Heyl, *Opt. Lett.* **2021**, 46, 4686.
- [17] R. H. Stolen, J. Botineau, A. Ashkin, *Opt. Lett.* **1982**, 7, 512.
- [18] H. J. Liu, Q. B. Sun, N. Huang, J. Wen, Z. L. Wang, *Opt. Lett.* **2013**, 38, 1838.
- [19] M. P. Kalashnikov, E. Risse, H. Schönnagel, A. Husakou, J. Herrmann, W. Sandner, *Opt. Express* **2004**, 12, 5088.
- [20] V. Pajer, M. Kalashnikov, *Laser Phys. Lett.* **2021**, 18, 065401.
- [21] T. R. Schibli, J. Kim, O. Kuzucu, J. T. Gopinath, S. N. Tandon, G. S. Petrich, L. A. Kolodziejski, J. G. Fujimoto, E. P. Ippen, F. X. Kaertner, *Opt. Lett.* **2003**, 28, 947.
- [22] S. Schulz, I. Grguraš, C. Behrens, H. Bromberger, J. T. Costello, M. K. Czwalińska, M. Felber, M. C. Hoffmann, M. Ilchen, H. Y. Liu, T. Mazza, M. Meyer, S. Pfeiffer, P. Prędki, S. Schefer, C. Schmidt, U. Wegner, H. Schlarb, A. L. Cavalieri, *Nat. Commun.* **2015**, 6.
- [23] M. Felber, E. Felber, M. Fenner, T. Kozak, T. Lamb, J. Müller, K. Przygoda, H. Schlarb, S. Schulz, C. Sydlo, M. Titberidze, F. Zummack, in *Proc. 39th Free Electron Laser Conf. FEL2019*, JACoW Publishing, Hamburg, Germany **2019**, p. 3.
- [24] S. Goloboroko, G. Grygiel, O. Hensler, V. Kocharyan, K. Rehlich, P. Shevtsov, in *ICALEPCS, IHEP, Beijing* **1997**, p. 141.
- [25] F. Peters, I. Hartl, C. Mohr, L. Winkelmann, in *Proc. 16th Int Conf Accel. Large Exp. Control Syst. ICALEPCS2017*, JACoW Publishing, Barcelona, Spain **2018**, p. 4.
- [26] S. Owada, M. Fushitani, A. Matsuda, H. Fujise, Y. Sasaki, Y. Hikosaka, A. Hishikawa, M. Yabashi, *J. Synchrotron Radiat.* **2020**, 27, 1362.
- [27] A. Azima, S. Düsterer, P. Radcliffe, H. Redlin, N. Stojanovic, W. Li, H. Schlarb, J. Feldhaus, D. Cubaynes, M. Meyer, J. Dardis, P. Hayden, P. Hough, V. Richardson, E. T. Kennedy, J. T. Costello, *Appl. Phys. Lett.* **2009**, 94, 144102.
- [28] G. Saathoff, L. Miaja-Avila, M. Aeschlimann, M. M. Murnane, H. C. Kapteyn, *Phys. Rev. A* **2008**, 77, 022903.
- [29] T. E. Glover, R. W. Schoenlein, A. H. Chin, C. V. Shank, *Phys. Rev. Lett.* **1996**, 76, 2468.
- [30] S. Meister, A. Bondy, K. Schnorr, S. Augustin, H. Lindenblatt, F. Trost, X. Xie, M. Braune, R. Treusch, B. Manschwetus, N. Schirmel, H. Redlin, N. Douguet, T. Pfeifer, K. Bartschat, R. Moshhammer, *Phys. Rev. A* **2020**, 102, 062809.

- [31] C. Behrens, N. Gerasimova, C. Gerth, B. Schmidt, E. A. Schneidmiller, S. Serkez, S. Wesch, M. V. Yurkov, *Phys. Rev. Spec. Top. - Accel. Beams* **2012**, 15, 030707.
- [32] M. Beye, FLASH2020+: Making FLASH Brighter, Faster and More Flexible: Conceptual Design Report (Deutsches Elektronen-Synchrotron, DESY, Hamburg, Germany **2020**.
- [33] P. Balla, A. Bin Wahid, I. Sytceovich, C. Guo, A.-L. Viotti, L. Silletti, A. Cartella, S. Alisauskas, H. Tavakol, U. Grosse-Wortmann, A. Schönborg, M. Seidel, A. Trabattori, B. Manschwetus, T. Lang, F. Calegari, A. Couaïron, A. L'Huillier, C. L. Arnold, I. Hartl, C. M. Heyl, *Opt. Lett.* **2020**, 45, 2572.
- [34] A.-L. Viotti, S. Alisauskas, A. Bin Wahid, P. Balla, N. Schirmel, B. Manschwetus, I. Hartl, C. M. Heyl, *J. Synchrotron Radiat.* **2021**, 28, 36.
- [35] G. Schönhense, D. Kutnyakhov, F. Pressacco, M. Heber, N. Wind, S. Y. Agustsson, S. Babenkov, D. Vasilyev, O. Fedchenko, S. Chernov, L. Rettig, B. Schönhense, L. Wenthaus, G. Brenner, S. Dziarzhyski, S. Palutke, S. K. Mahatha, N. Schirmel, H. Redlin, B. Manschwetus, I. Hartl, Y. Matveyev, A. Gloskovskii, C. Schlueter, V. Shokeen, H. Duerr, T. K. Allison, M. Beye, K. Rossnagel, et al., *Rev. Sci. Instrum.* **2021**, 92, 053703.
- [36] A. Jullien, O. Albert, F. Burgy, G. Hamoniaux, J.-P. Rousseau, J.-P. Chambaret, F. Augé-Rochereau, G. Chériaux, J. Etchepare, N. Minkovski, S. M. Saltiel, *Opt. Lett.* **2005**, 30, 920.
- [37] J. Itatani, J. Faure, M. Nantel, G. Mourou, S. Watanabe, *Opt. Commun.* **1998**, 148, 70.
- [38] H. C. Kapteyn, A. Szoke, R. W. Falcone, M. M. Murnane, *Opt. Lett.* **1991**, 16, 490.
- [39] R. W. Boyd, *Nonlinear Optics*, 4th ed., Academic Press, San Diego **2019**.
- [40] N. G. Khodakovskiy, M. P. Kalashnikov, V. Pajer, A. Blumenstein, P. Simon, M. M. Toktamis, M. Lozano, B. Mercier, Z. Cheng, T. Nagy, R. Lopez-Martens, *Laser Phys. Lett.* **2019**, 16, 095001.
- [41] K. Mecseki, M. K. R. Windeler, A. Miahnahri, J. S. Robinson, J. M. Fraser, A. R. Fry, F. Tavella, *Opt. Lett.* **2019**, 44, 1257.
- [42] G. Palmer, M. Kellert, J. Wang, M. Emons, U. Wegner, D. Kane, F. Pallas, T. Jezynski, S. Venkatesan, D. Rompotis, E. Brambrink, B. Monoszlai, M. Jiang, J. Meier, K. Kruse, M. Pergament, M. J. Lederer, *J. Synchrotron Radiat.* **2019**, 26, 328.
- [43] T. Lang, S. Alisauskas, U. Große-Wortmann, T. Hülsenbusch, B. Manschwetus, C. Mohr, J. Müller, F. Peters, N. Schirmel, S. Schulz, A. Swiderski, J. Zheng, I. Hartl, in 2019 Conf. Lasers Electro-Opt. Eur. Quantum Electron. Conf., Optical Society of America, Washington, DC **2019**, p. ca_2_1.
- [44] T. Togashi, S. Owada, Y. Kubota, K. Sueda, T. Katayama, H. Tomizawa, T. Yabuuchi, K. Tono, M. Yabashi, *Appl. Sci.* **2020**, 10, 7934.
- [45] C. Grebing, M. Müller, J. Buldt, H. Stark, J. Limpert, *Opt. Lett.* **2020**, 45, 6250.
- [46] M. Kaumanns, D. Kormin, T. Nubbemeyer, V. Pervak, S. Karsch, *Opt. Lett.* **2021**, 46, 929.
- [47] Y. Ma, S. Salman, C. Li, C. Mahnke, Y. Hua, S. Droste, J. Fellingner, A. Mayer, O. Heckl, C. Heyl, I. Hartl, *J. Light. Technol.* **2021**, 39, 4431.
- [48] T. Sato, R. Letrun, H. J. Kirkwood, J. Liu, P. Vagovič, G. Mills, Y. Kim, C. M. S. Takern, M. Planas, M. Emons, T. Jezynski, G. Palmer, M. Lederer, S. Schulz, J. Mueller, H. Schlarb, A. Silenzi, G. Giovanetti, A. Parenti, M. Bergemann, T. Michelat, J. Szuba, J. Grünert, H. N. Chapman, A. P. Mancuso, *Optica* **2020**, 7, 716.